Modeling and Displaying Dust Accumulation Process on Solar Panel and Impacts on Photoelectrical Conversion in a Virtual Reality Environment

Jian Ni[1], Mei Yang[1], Shengjie Zhai[1,2] and Yingtao Jiang[1,*]

Abstract: Dust accumulation on the surface of solar photovoltaic (PV) panels can significantly decrease the amount of solar irradiance reaching the cells, and consequently, can negatively impact the amount of electricity generated. In the literature, there have been quite a few theoretical or empirical studies to model the impacts of dust on solar power generation, but little has been done to "observe" and model the process of how dust gets to solar cells in the first place and appreciate the major ambient factors that are related to dust accumulation. This paper attempts to bridge that gap by building such a photoelectrical conversion model that immerses users into a virtual reality (VR) environment made of solar panels, sun radiation, and dust particles. In specific, the photoelectrical conversion of solar panels is modeled by taking into account of four contributing factors: 1) relationship between solar angle and light incidence angle; 2) the impact of environment parameters on the effective irradiance, including temperature, wind speed, sun position, date, geographical location of solar panels; 3) statistics of accumulated dust, dust accumulation rates, and the effect of accumulated dust on the panel; and 4) solar panel cell equivalent circuit. The real-world environmental hourly data, over the course of 20 years, obtained from National Renewable Energy Laboratory (NREL), are fit into the VR model, and the dust accumulation effects on solar electricity production can be visualized. This work clearly demonstrates how latest VR technologies can play a central role in manipulating and displaying a large amount data from long-term, complex, incomplete, and irregular data sets.

Key Words: Solar Panel, Dust Accumulation, Virtual Reality, Simulation.

Nomenclature

Air mass AM	Global Horizontal Irradiance GHI
Direct Normal Irradiance DNI	Plane of Array Irradiance (POA) G_{POA}
Diffuse Horizontal Irradiance DHI	Ground reflected component of POA G_r
Extraterrestrial radiation E_a	Absorbed irradiance G_S
Panel Efficiency Eff	Current I
Energy gap E_g	Incidence angle reflection losses IAM
Equation of time E_{qt}	Light current I_L
Solar Constant (1367W/m^2) E_{sc}	Voltage at max power point I_{mpp}
Beam component of POA G_b	Diode reverse saturation current I_o
Sky Diffuse Component of POA G_d	Short-circuit current I_{sc}

1. Department of Electrical and Computer Engineering, University of Nevada, Las Vegas, Nevada, USA. 89154
2. Department of Mechanical Engineering, University of Nevada, Las Vegas, Nevada, USA. 89154
*Corresponding Author: Yingtao Jiang. Email: yingtao.jiang@unlv.edu.

Boltzmann constant k
Diffuse Fraction K_d
Clearness Index K_t
Air mass modifier M
Diode ideality factor n
Nominal operating cell temperature $NOCT$
Maximum power P_{mpp}
Precipitable water P_{wat}
Electron charge q
Soiling Factor SF
Standard Rated Condition SRC
Series resistance R_s
Shunt resistance R_{sh}
Ambient temperature T_a
Cell temperature T_c
Module temperature T_m
Solar time T_{solar}
Voltage V
Current at max power point V_{mpp}
Open-circuit voltage V_{oc}
Wind speed W_s
Temperature coefficient for short-circuit current α_{Isc}
Temperature coefficient for max power α_{Pmpp}
Temperature coefficient for open-circuit voltage α_{Voc}
Azimuth angle θ_A
Incidence angle θ_{inc}
Tilt Angle θ_{tilt}
Zenith angle θ_Z

1. Introduction

Rapid advances in hardware and software in recent years has prompted the utilization of virtual reality (VR) technology in dental education[1], VR simulator for robotic surgery[2], Jaguar Land Rover virtual reality center in UK, and so on. These applications of VR mainly intend to take advantage of a friendlier interaction experience. As a matter of fact, VR can also be applied to help model and visualize complex processes. In this paper, we attempt to build a solar panel model with dust accumulation and visualize in a VR environment the performance of solar panel that is affected by many factors.

Solar photovoltaic (PV) panels have been widely used to generate electricity to power home and business. One of the major contributors of PV panel efficiency loss is the dust accumulated on the surface of PV panels[3,4], which can significantly decrease the amount of solar irradiation hitting solar cells. In the literature, there are several studies on building theoretical and/or empirical models to understand the impacts of dust on solar power generation. However, very few studies are conducted to "observe" and thus model the process of how dust gets to solar cells in the first place and investigate the major environmental factors that could impact dust accumulation. This paper aims to bridge the gap by building a PV solar panel model in a VR environment that must account for both the amount of accumulated dust and the continuing process of dust accumulation on a flat surface.

In order to design such an accurate VR model of solar panels that includes dust accumulation effects, we need to model these key factors: 1) relation of solar angle and incidence angle; 2) the impact of environment parameters (such as temperature, wind speed, sun position, date,

geographic location, accumulated dust on panel surface and so on) on the effective irradiance; 3) solar panel cell equivalent circuit.

De Soto came up with the five-parameter model for modeling solar cells [5]. Mohammed Asim demonstrated how to calculate and simulate the five-parameter model for a given solar panel parameters using manufacturer provided data[6]. An and Kumar showed how irradiance and on-board temperature affect solar panel performance[7]. Neil S. Beattie came up with a practical model about how dust get deposited on a panel surface[8]. The amount of accumulated dust over 2 years in a desert region could be seen in Goossens's work[9]. Ahmad Y. Al-hasan stated a relationship between PV panel's efficiency and the amount of accumulated dust on the panel surface[10].

In light of these aforementioned works, a theoretical integrated model of solar panel which accounts for multiple relevant environment parameters (such as temperature, wind speed, sun position, date, latitude, longitude, rate of dust accumulation on panel surface and so on) can be derived. To the best of our knowledge, we have included all the parameters that will affect the performance of the solar panel and the effects they have in the model. With these environmental data inputs, such an integrated model is built in a VR environment, as shown in figure 1, for the purposes of displaying and model tuning. The dynamic change of the performance (output power, current, voltage, efficiency, dust coverage, etc.) of the panel can be seen in an immersive view from the model.

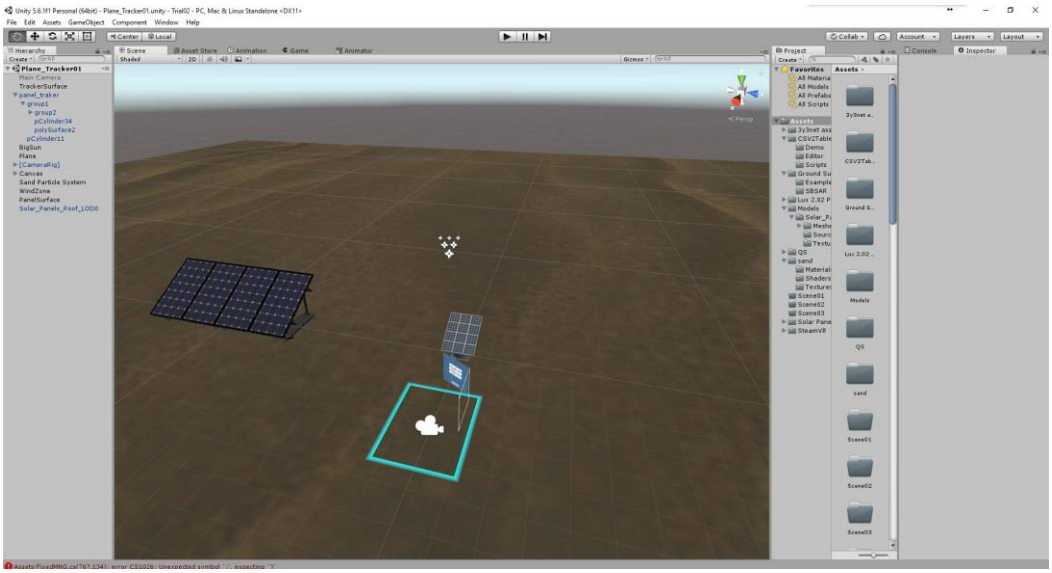

Figure 1. Solar panel model built in VR environment

The rest of this paper is organized as follows. Section 2 presents how dust particles accumulate on a flat surface. Sections 3 to 5 model the three major factors that affect the performance of solar panel. A comprehensive VR model that is built upon all the models described in Sections 3 through 5 is summarized in Section 6. The longitudes and latitudes of three major cities along with their hourly climate data from NREL[11,12] are employed to fit the proposed VR model. The simulation results of the chosen city based on solar panel electrical data and monthly dust

accumulation data from a study reported in Goossens's work[9] are also compared for model validation. Finally, in Section 7, conclusions are drawn.

2. Dust accumulation

According to Al-hasan's work[10], sand particles are modeled as a single layer of spheres of same sizes. When dust (sand) particles are accumulated on a flat surface, we can assume that they are uniformly and closely distributed on the surface. In this study, the diameter of sand particles is assumed to be 6.4um and density of sand to be 2.65g/cm^3.

If the surface has a tilt angle, the dust covered area as a function of the tilt angle is given as[10]:

$$A(\theta_{tilt}) = \frac{M}{\frac{4}{3}\pi\rho r^3}\pi r^2 * [\frac{1}{\tan(\frac{90-\theta_{tilt}}{2})} + \tan(\frac{90-\theta_{tilt}}{2})] \quad (1)$$

However, dust particles can accumulate on top of each other. That is, the single layer model may not match the measured data well. Based on Neil's work[8], a lower layer of sand cluster can support an upper layer of sand particles. As a result, a modified equation of dust accumulation with multiple layers is given as:

$$\frac{dA}{dM} = 1 - A \rightarrow A = 1 - e^{-M} \quad (2)$$

In our previous paper[13], we presented an improved multi-layer model for a fixed tilt angle surface as below:

$$A(\theta_{tilt}) = 1 - e^{-\frac{3M}{4\rho r} * [\frac{1}{\tan(\frac{90-\theta_{tilt}}{2})} + \tan(\frac{90-\theta_{tilt}}{2})]} \quad (3)$$

3. Solar Angle

Solar angle is one key parameter since it affects the incidence angle. Typically, solar angle can be divided into the Zenith angle and the Azimuth angle. These two angles are affected by the date, the latitude and the longitude of the observer's location.

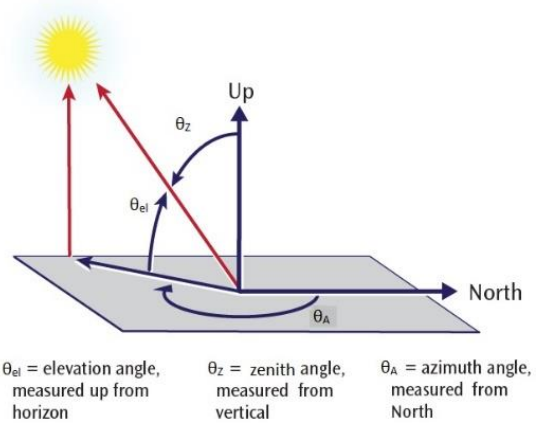

Figure 2. Zenith and Azimuth angle[14]

First, we consider the effect of the date. Earth is rotating around the sun. For every single day around the year, the angle between the Earth's rotation axis and the line connecting the centers of the Earth and the sun also changes. This angle is defined as the dayth angle, θ_d, shown in figure 2.

$$\theta_d = \frac{23.45\pi}{180}\sin(2\pi\frac{284+n}{365}) \tag{4}$$

During a day, the angle of the sun's orbit in the sky, denoted as the hourth angle, θ_{hourth} also changes with time. This angle is estimated on an hourly basis, and it sets to be 0 at solar noon, the time when the sun is at the highest point of its orbit in the sky of the day. A date influence factor, E_{qt}, has to be introduced to estimate the time of solar noon of a certain day over a year[15].

$$E_{qt} = \begin{cases} -14.2\sin(\frac{n+7}{111}\pi), n \in [1,106] \\ 4.0\sin(\frac{n-106}{59}\pi), n \in [107,166] \\ -6.5\sin(\frac{n-166}{80}\pi), n \in [167,246] \\ 16.4\sin(\frac{n-247}{113}\pi), n \in [247,365] \end{cases} \tag{5}$$

Note that the time of solar noon, T_{solar}, is also affected by both the local longitude and the longitude of the observer's location. Therefore,

$$T_{solar} = T_{local} + \frac{E_{qt}}{60} + \frac{Long_{tz} - Long_{local}}{15} \tag{6}$$

For the hourth angle, θ_{hourth}, we only need to consider when $\theta_{hourth} \in [0,\pi]$, which corresponds to the time when there is meaningful irradiance of a day for solar power production.

$$\theta_{hourth} = \frac{12 - T_{solar}}{12}\pi \tag{7}$$

Putting things together, we can obtain one solar angle, the Zenith angle as follows:

$$\theta_Z = \cos^{-1}(\sin(Lat_{local})\sin(\theta_d) + \cos(Lat_{local})\cos(\theta_d)\cos(\theta_{hourth})) \tag{8}$$

The other angle, the Azimuth angle, θ_A, is usually measured and given in the data record[16].

$$\theta_{inc} = \cos^{-1}(\cos(\theta_Z)\cos(\theta_{tilt}) + \sin(\theta_Z)\sin(\theta_{tilt})\cos(\theta_A - \theta_{A,array})) \tag{9}$$

The panel tilt angle, θ_{tilt}, is usually related to the latitude of the panel's geographical location.

The Azimuth angle of a solar array, $\theta_{A,array}$, is normally fixed. For instance, considering a solar panel facing south, θ_A is changing hourly, while $\theta_{A,array}$ is always set to be 180°.

4. Absorbed Irradiance

The absorbed irradiance by a solar panel has two components: the beam component G_b and the diffuse component. The diffuse component is a combination of ground reflected irradiance, G_r,

and sky-diffuse component, G_d. Furthermore, the sky-diffuse irradiance, G_d, is related to the extraterrestrial irradiance, E_a.

$$E_a = E_{sc} * (\frac{R_{av}}{R})^2 \tag{10}$$

Where solar constant $E_{sc} = 1367 W/m^2$; R_{av} is the average distance between the sun and the earth; and R is the distance between the sun and the earth for a given day.

For the sake of computation, E_a has the Taylor-series expansion. E_a is given below[14]

$$\begin{aligned} E_a = E_{sc} * [&1.00011 + 0.034221\cos(b) + 0.00128\sin(b) \\ &+0.000719\cos(2b) + 0.000077\sin(2b)] \end{aligned} \tag{11}$$

where (b in radians)

$$b = 2\pi \frac{n}{365} \tag{12}$$

Pyranometer is the most commonly used device to detect and record the radiation of different components of sun irradiance. Since a pyranometer is set to be placed horizontally to receive the sun light, the data recorded are direct normal irradiance, *DNI*, diffuse horizontal irradiance, *DHI*, and global horizontal irradiance, *GHI*.

Given the Zenith angle, any of the three data can be estimated from the other two in case there is one missing.

$$GHI = DNI * \cos(\theta_Z) + DHI \tag{13}$$

Two other useful parameters can also be obtained from measurements:

Sky clearness index: $K_t = \frac{GHI}{E_a}$

Diffuse fraction: $K_d = \frac{DHI}{GHI}$

However, for a panel with a tilt angle, adjustments of these parameters need to be made to account for the panel incidence irradiance, G_{POA}, the beam component of G_{POA}, G_b, the ground reflected component of G_{POA}, G_r, and the sky-diffuse component of G_{POA}, G_d.

From Lave's work[17], we have

$$G_{POA} = G_b + G_r + G_d \tag{14}$$

and

$$G_b = DNI * \cos(\theta_{inc}) \tag{15}$$

$$G_r = GHI * albedo * \frac{1 - \cos(\theta_{tilt})}{2} \tag{16}$$

$$G_d = DHI * \frac{1 + \cos(\theta_{tilt})}{2} + GHI * \frac{(0.012\theta_Z - 0.04) * (1 - \cos(\theta_{tilt}))}{2} \tag{17}$$

where *albedo* refers to the reflectivity of the ground surface, and its s values are tabulated in Table 1.

Table 1. *albedo* values for some interested environment[14]

Environment	Urban environment	Fresh grass	Concrete
albedo value	0.14~0.22	0.26	0.25~0.35

Note that not every single wavelength or a section of spectrum of the incidence irradiance will be absorbed by the panel cell. Certain spectrum of incidence light will not be absorbed by the cell due to the construct material used, some incidence light is reflected upon hitting the surface glass, and some incidence light is just blocked by the dust particles on the panel surface. Correspondingly, to determine the absorbed irradiance, G_S, we have to include a spectrum modifier, M, a reflection loss modifier, IAM, and a soiling factor, SF[14].

$$G_s = M*(IAM*G_b + G_r + G_d)*SF \tag{18}$$

Spectrum modifier M is related to the air mass (AM), and the precipitable water (P_{wat})[18]. Here AM depends on the Zenith angle[19].

$$AM = \frac{1}{\cos(\theta_Z) + 0.5057*(96.080 - \theta_Z)^{-1.684}} \tag{19}$$

$$M = f(AM, P_{wat}) = b_0 + b_1*AM + b_2*P_{wat} + b_3*\sqrt{AM} + b_4*\sqrt{P_{wat}} + b_5*\frac{AM}{\sqrt{P_{wat}}} \tag{20}$$

For both mono-Si and poly-Si cell, we shall have[18]

$b_0 = 0.8409, b_1 = -0.02754, b_2 = -0.00792,$

$b_0 = 0.1357, b_0 = 0.03802, b_0 = -0.002122.$

And the rated conditions to estimate M_{ref} are $P_{wat,ref} = 1.42cm, AM_{ref} = 1.5$.

Reflection loss modifier IAM is obtained based on Snell's Law[5].

$$\theta_{refl} = \sin^{-1}(\frac{1}{n_s}*\sin(\theta_{inc})) \tag{21}$$

$$IAM = \frac{\tau(\theta)}{\tau(0)} \tag{22}$$

$$\tau(\theta) = e^{-(\frac{KL}{\cos(\theta_{refl})})}*[1 - \frac{1}{2}(\frac{\sin^2(\theta_{refl} - \theta)}{\sin^2(\theta_{refl} + \theta)} + \frac{\tan^2(\theta_{refl} - \theta)}{\tan^2(\theta_{refl} + \theta)})] \tag{23}$$

$$\tau(0) = \lim_{\theta \to 0}\tau(\theta) = e^{-KL}*[1 - \left(\frac{1 - n_s}{1 + n_s}\right)^2] \tag{24}$$

It is suggested to choose the following values for glass medium to calculate IAM[5]:

$K = 4m^{-1}, L = 0.002m, n_s = 1.526$.

Note that this modifier can only be applied to the beam component.

For soiling factor SF, in this paper, we only consider the soiling source that is the accumulated dust on the panel surface. As we discussed in Section 2, when considering the impact of the accumulated dust on panel surface in terms of the panel performance, we assume that the covered

area blocks all the incidence light. That means for unit area, the ratio of covered area equals to the percentage loss of the incidence irradiance. That is,

$$SF = 1 - A(\theta_{tilt}) \tag{25}$$

5. Solar Cell Equivalent Circuit

When considering electrical parameters of a solar panel, cell temperature, T_c, has to be the very first parameter to deal with, since the performance of a solar cell is so much dependent on the cell temperature. In general, T_c is affected by ambient temperature, the wind speed, and the incidence irradiance[20].

$$T_c = T_a + \frac{G_{POA}}{U_0 + U_1 * W_s} \tag{26}$$

where $U_0 = 25W/m^2K$ and $U_0 = 6.84W/m^3sK$.

Next, we consider the equivalent circuit of a single solar cell, as drawn in figure 3.

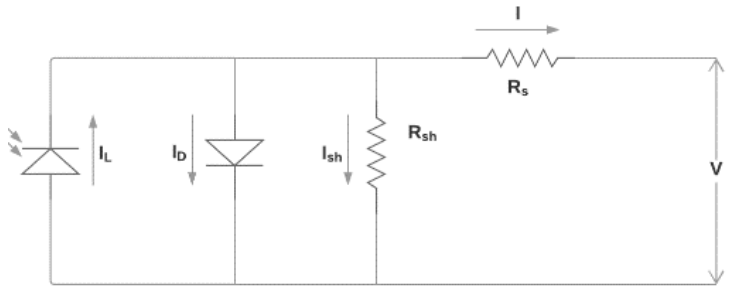

Figure 3. Equivalent circuit of a single solar cell

For this circuit, simple circuit analysis will reveal that

$$I = I_L - I_o[e^{\frac{V+I*R_s}{\alpha}} - 1] - \frac{V + I*R_s}{R_{sh}} \tag{27}$$

The short circuit current, the open circuit voltage, and the maximum power-transfer point, are given below

$$I_{sc,ref} = I_{L,ref} - I_{o,ref}[e^{\frac{I_{sc,ref}*R_{s,ref}}{\alpha_{ref}}} - 1] - \frac{I_{sc,ref} * R_{s,ref}}{R_{sh,ref}} \tag{28}$$

$$0 = I_{L,ref} - I_{o,ref}[e^{\frac{V_{oc,ref}}{\alpha_{ref}}} - 1] - \frac{V_{oc,ref}}{R_{sh.ref}} \tag{29}$$

$$I_{mpp} - V_{mpp}\frac{-\frac{I_o}{\alpha}e^{\frac{V_{mpp}+I_{mpp}*R_s}{\alpha}} - \frac{1}{R_{sh}}}{1 + \frac{I_o * R_s}{\alpha}e^{\frac{V_{mpp}+I_{mpp}*R_s}{\alpha}} + \frac{R_s}{R_{sh}}} = 0 \tag{30}$$

By plugging in the parameter data provided by solar panel manufacturer (usually given in terms of $I_{sc,ref}$, $V_{oc,ref}$, $P_{mpp,ref}$, $I_{mpp,ref}$, $V_{mpp,ref}$) as tabulated in Table 2, we can obtain $I_{L,ref}$ and $I_{o,ref}$ in Eqns. (28) and (29).

Table 2. Key performance data provided by SunPower of its E-Series Commercial Solar Panel E20-435 (from the data sheet)

Electrical Data		
Parameters	**SPR-E20-435-COM**	**SPR-E19-410-COM**
Nominal Power (P_{nom})	435W	410W
Power Tolerance	+/-5%	+/-5%
Avg. Panel Efficiency	20.3%	19.1%
Rated Voltage (V_{mpp})	72.9V	72.9V
Rated Current (I_{mpp})	5.97A	5.62A
Open-Circuit Voltage (V_{oc})	85.6V	85.3V
Short-Circuit Current (I_{sc})	6.43A	6.01A
Max. System Voltage	1000V UL & 1000 V IEC	
Maximum Series Fuse	15A	
Power Temp Coef.	-0.35%/℃	
Voltage Temp Coef.	-235.5mV/℃	
Current Temp Coef.	2.6mA/℃	

When $I_{L,ref}$ and $I_{o,ref}$ are obtained, we can get I_L and I_o at any cell temperature within the operating interval of Eqns. (31) and (32). Then, substituting them into Eqn. (27), we can get the *I-V* curve at a certain condition, which corresponds to the performance of the panel at the specified condition.

$$I_L = \frac{G_s}{G_{ref}} \frac{M}{M_{ref}} [I_{L,ref} + \alpha_{Isc}(T_c - T_{c,ref})] \tag{31}$$

$$I_o = I_{o,ref} * (\frac{T_c}{T_{ref}})^3 * e^{[\frac{1}{k}(\frac{E_g(T_{ref})}{T_{ref}} - \frac{E_g(T_c)}{T_c})]} \tag{32}$$

$$E_g(T_c) = E_g(T_{c,ref})[1 - 0.0002677(T_c - T_{ref})] \tag{33}$$

$$R_s = R_{s,ref} \tag{34}$$

$$R_{sh} = R_{sh,ref} \frac{G_{s,ref}}{G_s} \tag{35}$$

$n = \text{constant} \in [1, 2]$

Modified diode ideality factor is typically given as

$$\alpha = \frac{N_s * n * k * T_c}{q} \tag{36}$$

For this factor α , we can just assume the number of cell is 1 and choose *n* to be 1.

De Soto assumed R_s independent of cell temperature in his Model[5]. For mono-silicon cell,

$R_{s,ref} = 0.969\Omega$, which is assumed as a constant at its reference value.

$R_{sh,ref} = 199\Omega$, which is inverse to the absorbed irradiance.

In Eqns. (27) and (30) at the maximum power-transfer point, using a nonlinear solver, we can always obtain the values of I_{mpp} and V_{mpp} for some specific condition, after which we will be able to determine the corresponding maximum power-transfer point P_{mpp} for that specific condition.

In this study, we ignore the wire losses and DC to AC converter model in VR, which can be accounted with a California Energy Commission (CEC) efficiency (typically 94.5%)[14]. With this said, we can evaluate the output efficiency as

$$Eff = \frac{0.945 * I * V}{G_{POA} * 1} * 100\% \tag{37}$$

6. Simulation Result and VR Creation

The VR simulation model of solar panels with the effect of dust accumulation is developed in Unity platform[21] and demonstrated using HTC Vive VR system[22]. The selected theoretical models of PV panels are coded into C# scripts to support the calculation of the real-time changes of the model parameters.

We look at three typical locations (Las Vegas, Chicago, New York City) with different climate conditions. The environmental data sets were collected from National Renewable Energy Laboratory (NREL)[11,12], which include the hourly climate data from 1991 to 2010 (including zenith angle, azimuth angle, latitude, longitude, wind speed, air mass, ambient temperature, extraterrestrial irradiance, direct normal irradiance, diffuse horizontal irradiance, global horizontal irradiance, albedo, precipitable water etc.). The electronic parameter sheet is from a commercial solar panel[23]. Another data set used is the monthly dust accumulation rate in a desert region[9].

With the integrated model and data sets, we can evaluate the performance of solar panel in VR environment.

6.1. I-V curve under some certain fixed conditions

When the absorbed irradiance, the ambient temperature and the incidence angle are fixed, we can get an *I-V* curve by sweeping the voltage from 0 to V_{oc} with Eqn. (27).

Model: Angle fixed model without dust accumulation (*SF* = 1)

Observer's Location: Las Vegas

1.) Date: 01/01/2010 10:00 am:

Corresponding Parameters: $T_c = 20.3^{\circ}C$, $\theta_{inc} = 51.28^{\circ}$, $G_{POA} = 353.4W/m^2$, $G_s = 255.6W/m^2$, $I_L = 2.5623A$, $I_o = 0.4699A$, $K_t = 0.5463$, $K_d = 0.6645$;

2.) Date: 03/03/2010 11:00 am;

Corresponding Parameters: $T_c = 36.3^{\circ}C$, $\theta_{inc} = 28.65^{\circ}$, $G_{POA} = 944.6W/m^2$, $G_s = 933.9W/m^2$, $I_L = 6.1149A$, $I_o = 0.5478A$, $K_t = 0.7848$, $K_d = 0.0820$;

3.) Date: 05/05/2010 11:00 am;

Corresponding Parameters: $T_c = 43.5^{\circ}C$, $\theta_{inc} = 38.05^{\circ}$, $G_{POA} = 770.0W/m^2$, $G_s = 747.8W/m^2$, $I_L = 4.8266A$, $I_o = 0.5866A$, $K_t = 0.6902$, $K_d = 0.5845$;

4.) Date: 06/06/2010 12:00 pm.

Corresponding Parameters: $T_c = 55.0^{\circ}C$, $\theta_{inc} = 15.85^{\circ}$, $G_{POA} = 1022.2W/m^2$, $G_s = 1009.3W/m^2$, $I_L = 6.6391A$, $I_o = 0.6530A$, $K_t = 0.7972$, $K_d = 0.1004$.

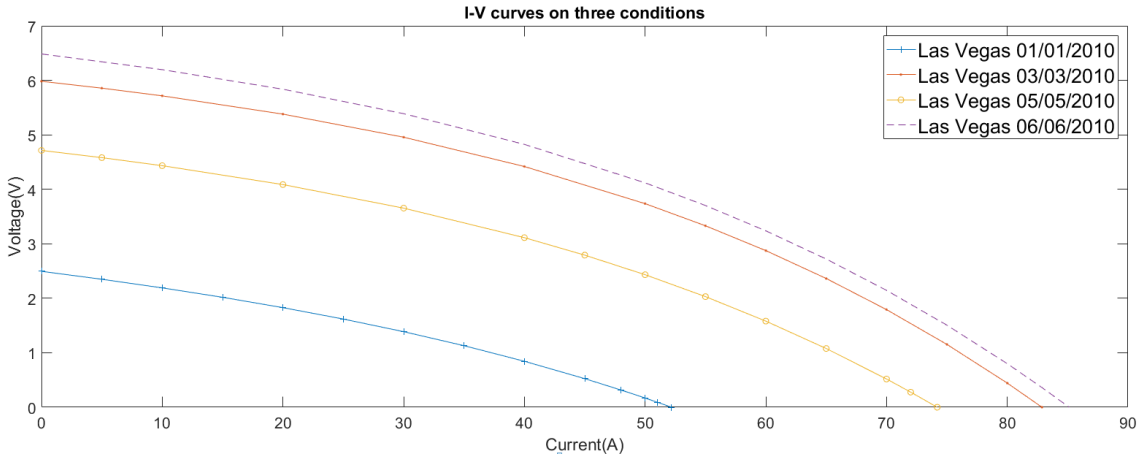

Figure 4. I-V curves for mono-Si type cell generated in VR for three operation conditions

From Fig. 4, the panel has a good efficiency around 19.8% at 03/03/2010 and 20.1% at 06/06/2010, which is due to the high absorbed irradiance. However, the panel still has a low efficiency around 11.8% at 01/01/2010 and 16.3% at 05/05/2010, which is due to bad weather and low absorbed irradiance.

6.2. Efficiency curve with variation of dust coverage

For angle fixed panel, in Las Vegas, on 08/01/2010 at 12:00 pm, variations of normalized efficiency and covered area versus the amount of accumulated dust are demonstrated in figure 5, according to Eqns. (3) and (37).

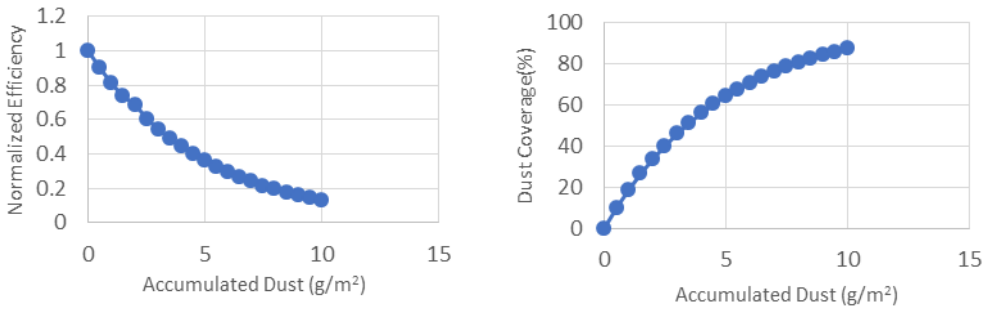

Figure 5. Variations of normalized efficiency and dust coverage with accumulated dust based on the modified model

Figure 6 shows the normalized efficiency of multi-layer dust model compared with that of Al-hasan's. In Fig. 6, the normalized efficiency of multilayer model decays slower than that of single layer model, which can be attributed to the fact that for the same amount of accumulated dust, the area covered by dust is less as predicted by the multilayer model than the single layer model with the same amount of accumulated dust.

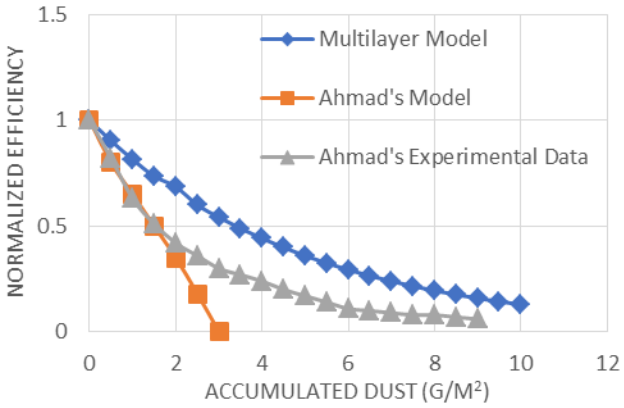

Figure 6. Comparison of the normalized efficiency as predicted by the multilayer model and the single layer model

A more visible change on the solar panel surface with different percentage of dust coverage can be seen in figure 7. A more immersive 3D view of the real-time dust accumulation process and electricity production can be observed while wearing the HTC Vive goggle.

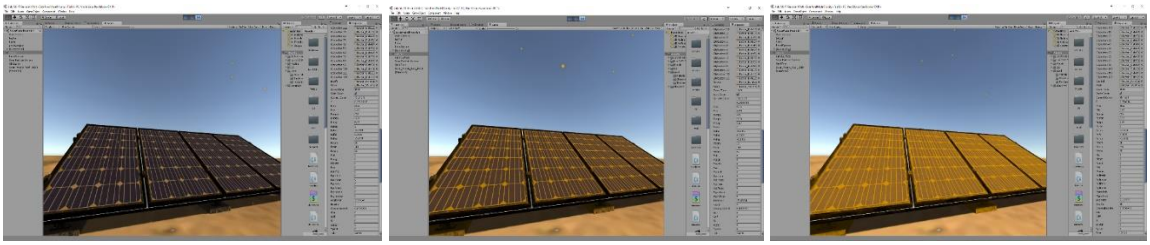

(a) (b) (c)

Figure 7. Solar panel with different amounts of dust on the suffice: (a) 5% surface covered by dust; (b) 20% surface covered by dust; (c) 80% surface covered by dust.

6.3. Comparison of the outputs between fixed angle panel and angle tracker panel

When the panel tilt angle is fixed, it's easy to fit the data into the integrated model. That's because the model is set for the situation when the panel has a tilt angle. However, for the panels that are designed to track the sun orbit in the sky in two axes, some modification of the original model is necessary.

1.) For a two-axis tracking panel, the surface is supposed to stay perpendicular to the incidence direction of the beam irradiance. In other words, θ_{tilt} is tracking θ_Z and $\theta_{A,array}$ is tracking θ_A. Thus, we can obtain

$$\theta_{tilt} = \theta_Z \tag{38}$$

and Eqn. (9) now becomes

$$\theta_{inc} = \cos^{-1}(\cos(\theta_Z)\cos(\theta_Z) + \sin(\theta_Z)\sin(\theta_Z)\cos(\theta_A - \theta_A)) = 0 \tag{39}$$

That is, the incidence angle is 0 indicating that none of beam irradiance is reflected, and the incidence reflection loss modifier is 1. Correspondingly, Eqn. (18) becomes:

$$G_s = M*(G_b + G_r + G_d)*SF \tag{40}$$

2.) For the tracker, since θ_Z varies from 90° sunrise, to minimum $\theta_{Z,\min}$ solar noon, then back to 90° at sunset, the panel tilt angle θ_{tilt} rises in the same way. However, for the dust accumulation model, it brings a concern here if the accumulated dust particles will fall with a large tilt angle. However, it was found that all these particles are not affected by gravity but Van der Waals force[24]. As a result, we can still use the same multi-layer model as presented in Section 3.

With all the modifications as described above, we make a comparison of the absorbed irradiance and efficiency obtained from the fixed angle model and the tracking angle model with Eqns. (18) (37) and (40).

Model: Fixed Angle Model and Tracking Angle Model

Observer's Location: Las Vegas

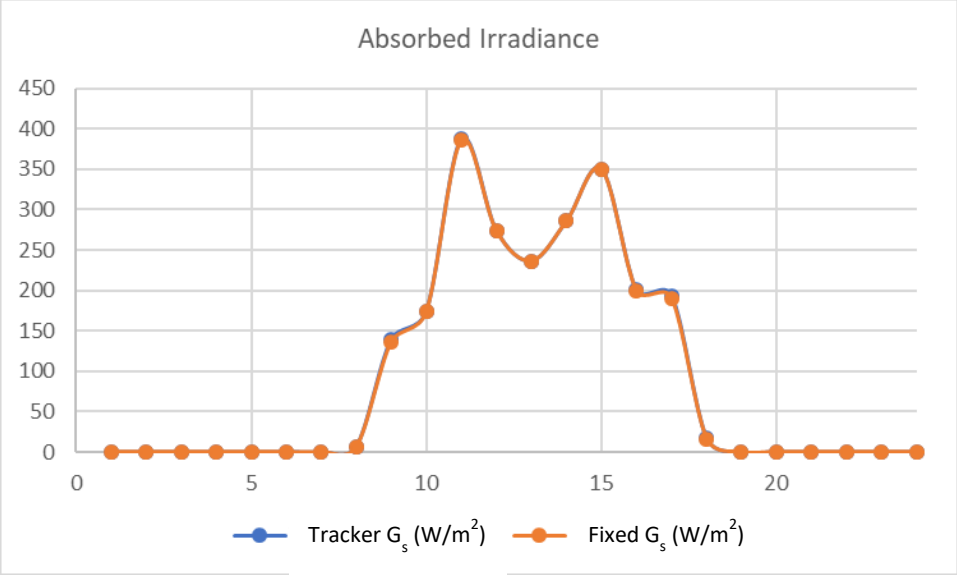

(a) Date: 01/01/2010 1:00 ~ 24:00;

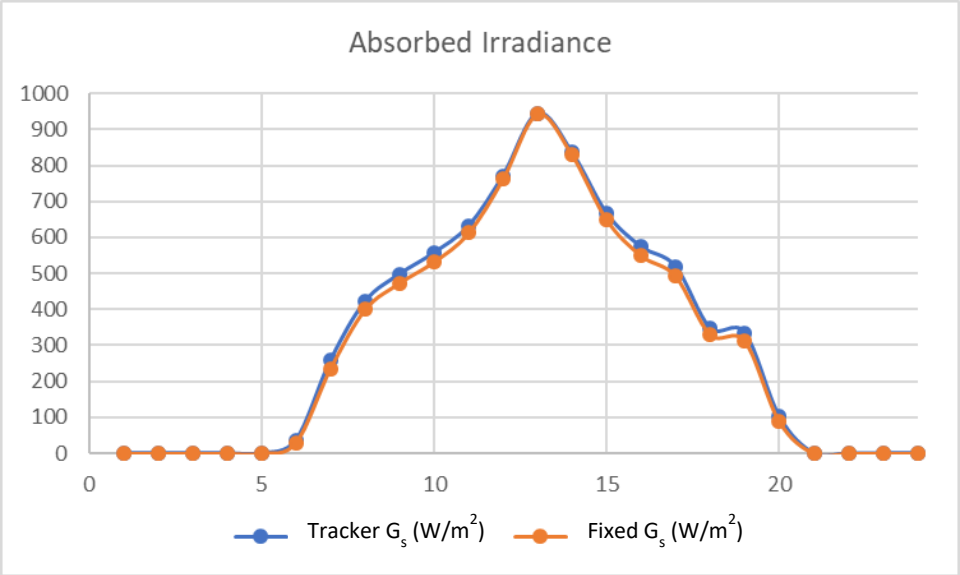

(b) Date: 06/06/2010 1:00 ~ 24:00;

Figure 8. Comparison of absorbed irradiance predicted by the fixed angle vs. that by the tracking model:

(a)01/01/2010; (b)06/06/2010

In figure 8(a), the weather condition was not good, and the beam irradiance was low for the entire day. The irradiance absorption determined by the fixed angle model is very close to the irradiance absorption predicted by the tracking angle model. In figure 8(b), the beam component was high. Compared with the fixed angle model, the tracking angle model actually predicts that all the beam irradiance was indeed absorbed, in better agreement with the measured data. Overall speaking, one can see that irradiance absorption determined by the tracking angle model is more accurate than that by the fixed angle model.

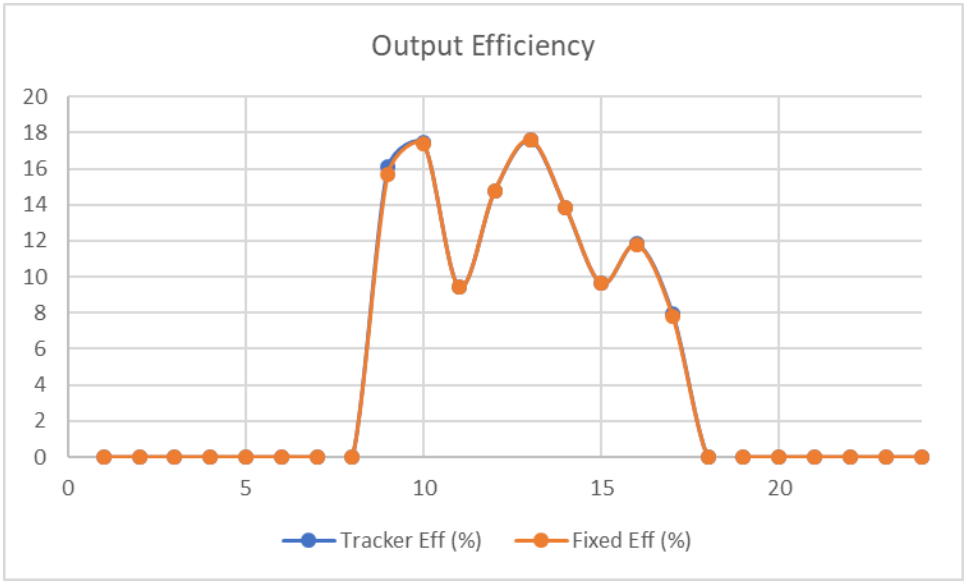

(a) Date: 01/01/2010 1:00 ~ 24:00;

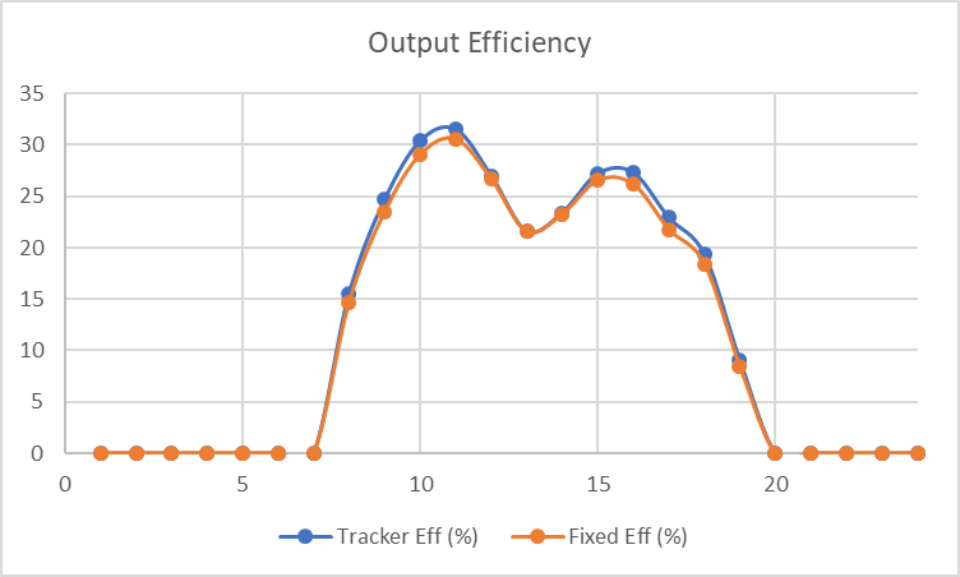

(b) Date: 06/06/2010 1:00 ~ 24:00;

Figure 9. Comparison of output efficiency as predicted by the fixed angle vs. that by the tracking model:

(a)01/01/2010; (b)06/06/2010

In figure 9(a), the weather condition was not good, and the beam irradiance was found to be low for the entire day. The output power predicted by the fixed angle model is very close to the power predicted by the tracking angle model. In figure 9(b), one can see the efficiency improvement due to the enhanced light current I_L produce in the tracking angle model. And when at around 12 pm, efficiency as predicted by the fixed angle model was close to that by the tracking angle model, which is due to the minimum incidence angle at solar noon.

7. Conclusions

This paper presented a solar panel model that accounts for dust accumulation in a virtual reality environment. The simulation results of the chosen city based on solar panel electrical data and monthly accumulated dust data were presented to let user visually see the real-time operation of the solar panel. The built VR solar panel model provided a convenient tool and method for designers to analyze and validate the important panel performance parameters pertaining to photoelectrical conversion.

Acknowledgment

The authors would like to thank NREL for providing the climate data of Las Vegas, Chicago and New York City. This work was supported in part by the National Science Foundation under Grant No. IIA-1301726.

References

1. **E. Roy, M. M. Bakr, and R. George**, "The need for virtual reality simulators in dental education: A review," Saudi Dent. J. **29**(2), 41–47 (2017).
2. **P. A. Kenney, M. F. Wszolek, J. J. Gould, J. A. Libertino, and A. Moinzadeh**, "Face, Content, and Construct Validity of dV-Trainer, a Novel Virtual Reality Simulator for Robotic Surgery," Urology **73**(6), 1288–1292 (2009).
3. **M. Mani and R. Pillai**, "Impact of dust on solar photovoltaic (PV) performance: Research status, challenges and recommendations," Renew. Sustain. Energy Rev. **14**(9), 3124–3131 (2010).
4. **J. K. Kaldellis and M. Kapsali**, "Simulating the dust effect on the energy performance of photovoltaic generators based on experimental measurements," Energy **36**(8), 5154–5161 (2011).
5. **W. De Soto, S. A. Klein, and W. A. Beckman**, "Improvement and validation of a model for photovoltaic array performance," Sol. Energy **80**(1), 78–88 (2006).
6. **M. Asim**, "Modelling and Simulation of 5 Parameter Model of Solar Cell Modelling and Simulation of 5 Parameter Model of Solar Cell," Int. J. Electr. Electron. Comput. Syst. **4**(July), 2–7 (2016).
7. **A. G. Acharya, S. Nawaz, and B. M. Patel**, "Analysis of Variation in Solar Panel Parameter with respect to Solar Isolisation and temperature," Int. J. Sci. Eng. Res. **3**(9), 1–6 (2012).
8. **N. S. Beattie, R. S. Moir, C. Chacko, G. Buffoni, et al.**, "Understanding the effects of sand and dust accumulation on photovoltaic modules," Renew. Energy **48**, 448–452 (2012).
9. **D. Goossens and Z. Y. Offer**, "Comparisons of day-time and night-time dust accumulation in a desert region," J. Arid Environ. **31**(3), 253–281 (1995).
10. **A. Y. Al-hasan and A. A. Ghoneim**, "A new correlation between photovoltaic panel's efficiency and amount of sand dust accumulated on their surface," Int. J. Sustain. Energy **24**(4), 187–197 (2005).
11. **NREL**, "National Solar Radiation Database 1991 – 2010 Update : User ' s Manual," 479 (2012).
12. **NREL**, "Solar Radiation Data Manual for Flat-Plate and Concentrating Collectors" (accessed 4 March 2018).
13. **J. Ni, M. Yang, and Y. Jiang**, "Virtual Reality Simulation of Dust Accumulation on the Surface of Solar Panel," Proc. - ICCSEC (2017).
14. **Sandia**, "PV Performance Modeling Collaborative | An Industry and National Laboratory collaborative to improve Photovoltaic Performance Modeling" (accessed 4 March 2018).
15. **I. Reda, A. Andreas, and A. A. Nrel**, "Solar Position Algorithm for Solar Radiation Applications (Revised)," Nrel/Tp-560-34302(January), 1–56 (2008).
16. **I. Reda and A. Andreas**, "Solar position algorithm for solar radiation applications," Sol. Energy **76**(5), 577–589 (2004).
17. **M. Lave, W. Hayes, A. Pohl, and C. W. Hansen**, "Evaluation of global horizontal irradiance to plane-of-array irradiance models at locations across the United States," IEEE J. Photovoltaics **5**(2), 597–606 (2015).

18. **M. Lee and A. Panchula**, "Spectral correction for photovoltaic module performance based on air mass and precipitable water," 43rd IEEE 43rd Photovolt. Spec. Conf., 1351–1356 (2016).

19. **D. L. King, J. A. Kratochvil, W. E. Boyson, and W. I. Bower**, "Field Experience With a New Performance Procedure for Arrays," Sol. Energy(July) (1998).

20. **D. Faiman**, "Assessing the outdoor operating temperature of photovoltaic modules," Prog. Photovoltaics Res. Appl. **16**(4), 307–315 (2008).

21. **Unity**, "Unity" (accessed 4 March 2018).

22. **HTC VIVE**, "VIVE™ | Discover Virtual Reality Beyond Imagination" (accessed 4 March 2018).

23. **SunPower**, "E-Series Commercial Solar Panels."

24. **J. VISSER**, "PARTICLE ADHESION AND REMOVAL: A REVIEW," Part. Sci. Technol. **13**(3–4), 169–196 (1995).

